The role of ELM filaments in setting the ELM wetted area in MAST and the implications for future devices

AJ Thornton[1], SY Allan[1], BD Dudson[2], SD Elmore[1], GM Fishpool[1], JR Harrison[1], A Kirk[1], the MAST Team and the EUROfusion MST1 Team*

[1]CCFE, Culham Science Centre, Abingdon, Oxon, OX14 3DB, UK
[2]York Plasma Institute, Department of Physics, University of York, Heslington, York, YO10 5DD, UK

E-mail: andrew.thornton@ukaea.uk

Abstract. The ELM wetted area is a key factor in the peak power load during an ELM, as it sets the region over which the ELM energy is deposited. The deposited heat flux at the target is seen to have striations in the profiles that are generated by the arrival of filaments ejected from the confined plasma. The effect of the filaments arriving at the target on the ELM wetted area, and the relation to the midplane mode number is investigated in this paper using infrared (IR) thermography and high speed visible imaging (>10kHz). Type I ELMs are analysed, as these have the largest heat fluxes and are observed to have toroidal mode numbers of between 5 and 15. The IR profiles during the ELMs show clear filamentary structures that evolve during the ELM cycle. An increasing number of striations at the target is seen to correspond to an increase in the wetted area. Analysis shows that the ratio of the ELM wetted area to the inter-ELM wetted area, a key parameter for ITER, for the type I ELMs is between 3 and 6 for lower single null plasmas and varies with the ELM midplane mode number, as determined by visible measurements. Monte-Carlo modelling of the ELMs is used to understand the variation seen in the wetted area and the effect of an increased mode number; the modelling replicates the trends seen in the experimental data and supports the observation of increased toroidal mode number generating larger target ELM wetted areas. ITER is thought to be peeling unstable which would imply a lower ELM mode number compared to MAST which is peeling-ballooning unstable. The results of this analysis suggest that the lower n peeling unstable ELMs expected for ITER will have smaller wetted areas than peeling-ballooning unstable ELMs. A smaller wetted area will increase the level of ELM control required, therefore a key prediction required for ITER is the expected ELM mode number.

*For full list of contributors, see http://www.euro-fusionscipub.org/mst1

PACS numbers: 52.55.Fa, 52.55.Rk, 52.70.-m, 52.65.Pp

Submitted to: *Plasma Phys. Control. Fusion*

7 September 2016

1. Introduction

The heat flux to the divertor during ELMs is a key issue for ITER due to the short duration and high intensity loads that they generate [1]. The ELM heat load can limit the operational lifetime of future devices due to damage to the divertor and as a result a means of ELM control is required [2]. A key parameter for ITER in the scaling of the ELM heat load is the ratio of the ELM to inter-ELM wetted area, as this sets the divertor area over which the ELM energy is deposited and correspondingly affects the level of control required to reduce the ELM heat load to tolerable levels [3]. It has been observed via fast imaging [4] and confirmed via simulation [5] that the ELM ejects a number of filaments from the midplane of the plasma. The number of filaments ejected is governed by the mechanism which drives that ELM unstable; with peeling unstable ELMs exhibiting the lowest toroidal mode numbers and ballooning unstable ELMs the highest [6]. The filaments travel from the plasma edge, depositing heat and particles to the target during their motion [7] which results in the formation of striations in the target profiles which were first observed on ASDEX-Upgrade [8, 9] and subsequently on MAST [7], DIII-D [10] and JET [11]. In addition to the filament motion, the filaments have been observed to carry a current and leading to ergodisation of the flux tube defined by the filament [12]. Generally, the ELMs in MAST are convective in nature for pedestal temperatures below 150 eV, therefore it would be expected that the profiles can be generated by considering the motion of ELM filaments over the ergodisation effects [13]. The ergodisation and the filament motion both contribute to the overall strike point pattern seen on the divertor target. Recent analysis from NSTX has shown that the number of striations in the divertor profiles affects the ratio of the ELM to inter-ELM wetted area [14]. Therefore, as the ELM mode number may differ in ITER compared to present devices, understanding of how the ratio of the ELM to inter-ELM wetted area scales with the toroidal mode number is key to predicting the ITER ELM wetted area.

This paper aims to investigate the effect of the ELM toroidal mode number has on the wetted area at the target using IR thermography and visible imaging. Type I ELMs on MAST have mode numbers of the order n=7-20 as measured using fast visible imaging at the midplane [15], suggesting that the MAST pedestal is peeling-ballooning mode unstable. In addition to direct measurement of the ELM toroidal mode number at the midplane, striations in the IR target profiles can be mapped to the midplane and a mode number determined which can be compared to the visible data [16]. The paper first investigates IR measurements of the ELMs in MAST in section 2 before generating a database of ELMs for analysis in section 3. The properties of the ELMs at the target are then extracted and compared to the midplane in section 5. The scaling between the number of filaments seen at the target and the ELM wetted area is investigated in section 5 and then interpreted using modelling in section 6.

2. IR measurements of the ELM target footprint in MAST

Understanding the evolution of the target heat flux due to an ELM on MAST can be gained by considering a single ELMy discharge and using this discharge to extract key ELM parameters and timescales. The example discharge here is MAST discharge 30378 which is a 400 kA lower single null plasma, heated with 3.4 MW of neutral beam injection, containing 25 type I ELMs. The divertor heat flux from ELMs is measured at the lower outer divertor using a medium wavelength (4.5-5.0 μm) infrared (IR) camera operated at 5 kHz, with an integration time of 28 μs and viewing the divertor at a spatial resolution of 1.5 mm per pixel. In order to measure at this frame rate, the camera is operated with a 320 pixel wide window in the radial direction and an 8 pixel wide window in the toroidal direction. As a result, the total toroidal coverage of the divertor target measured by the camera is of the order 0.5 degrees in the toroidal direction. The heat flux to the target determined from the measured surface temperature evolution using the inverse heat conduction code THEODOR [17], including a surface layer parameter of between 70 and 140 kW m^{-2} K^{-1}, which is determined by energy balance and consistency of ELM heat flux across the divertor for ELMs of the same energy. An example of an ELM captured using the IR camera is show in figure 1 a) which shows the time evolution of the divertor heat flux along the abscissa and the spatial extent along the ordinate. The increased heat flux from the ELM along with the characteristic broadening of the ELM footprint can be seen at the target in a). Panel b) shows a comparison of a profile taken at the peak of the ELM heat flux and one during an inter-ELM period, normalised to the peak heat flux. The data in figure 1 show a clear increase in both the width and magnitude of the heat flux to the divertor during the ELM.

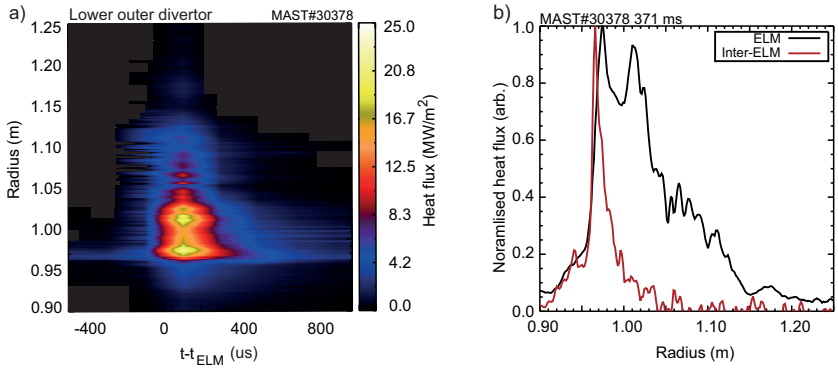

Figure 1. Contour plot of the heat flux from an ELM shown in a), where the abscissa corresponds to the time during the discharge, normalised to the midplane ELM D_α emission and the ordinate is the target radial position. Panel b) shows a profile taken at the peak of the ELM heat flux and one taken 1 ms prior to the ELM during an inter-ELM period.

Visible midplane imaging of ELMs has shown that the ELM filaments dwell at the edge of the plasma following formation and then move out across the SOL [18]. The

timescale over which the particles arrive at the divertor target is set by the motion of the particles along the magnetic field and is consistent with parallel propagation at the ion sound speed. The temporal evolution of ELMs in MAST can be characterised using the 25 ELMs in discharge 30378. In this discharge several ELMs are combined in time to generate a composite ELM showing the evolution of the heat flux to the target as a function of time through the ELM. To generate the composite ELM, the D_α from the 25 ELMs is used to align the ELMs in time; the peak of the emission is taken to be t=0 and the amplitude of the signal is normalised to 1 at this time, as shown in figure 2 a). The data in figure 2 a) shows that each these ELMs have similar rise and fall times (black dots). A time average of all of the data can be taken to produce the red solid line shown in the figure which highlights the rapid ELM rise and subsequent decay. By using the t=0 point defined using the Dα data, other properties of the ELM can be assessed to see how they vary in time. Figure 2 b) shows that the peak in the heat flux at the target is of the order 150-200 μs after the increase in light at the midplane, corresponding to the parallel transit time of ions at the pedestal temperature from the midplane to the divertor. The ELM wetted area can be calculated using the total power to the divertor, P_{tot}, and the peak heat flux q_{peak}. The total power is calculated using the integral over the ELM profile as given by;

$$P_{tot} = 2\pi \int q(r) r dr \tag{1}$$

where r is the radial location at the target and $q(r)$ is the radial heat flux profile. In the case of the ELM heat load, the integral is taken across the whole of the measured profile. Generating a wetted area for the inter-ELM profiles is required to assess the broadening that occurs during the ELM. For inter-ELM heat flux profiles the power to the target is calculated over only the region around the peak of the heat flux. The region is determined by fitting an exponential to the SOL side of the heat flux profile; using 3 times the fall off of this exponential on the private flux region (PFR) and 4 target fall off lengths on the SOL side as the radial range of the integral which represents the region over which the inter-ELM power decays to the background level. Extending the integral beyond this range causes noise to be included from regions where there is no heat flux. Once the value of P_{tot} is calculated, the wetted area, A_{wet} is calculated as $A_{wet} = P_{tot}/q_{peak}$ [14]. Previous methods used to calculate the wetted area involve the integral of the heat flux in time as well as space [19, 20] which adds uncertainty both on the definition of the start and end of the ELM and to the radial extent of the ELM heat flux. The resulting values for A_{wet} using the method by Jachmich et al [19] gives values of the order half those given by the method used in this paper but result in similar trends.

The temporal evolution of the ELM wetted area for the ELMs in discharge 30378 is shown in figure 2 c) for the corresponding peak heat fluxes shown in panel b). The ELM wetted area can be seen to increase as the ELM peak power load increases, consistent with the increase in the broadening of the profile seen in figure 1. The wetted area is

seen to increase from the inter-ELM level of 0.3 m^2 to 0.7 m^2 during the ELM, which is a 2.3 fold increase in the wetted area. The data in figure 2 shows that the maximum wetted area at the target coincides with the peak heat flux to the target.

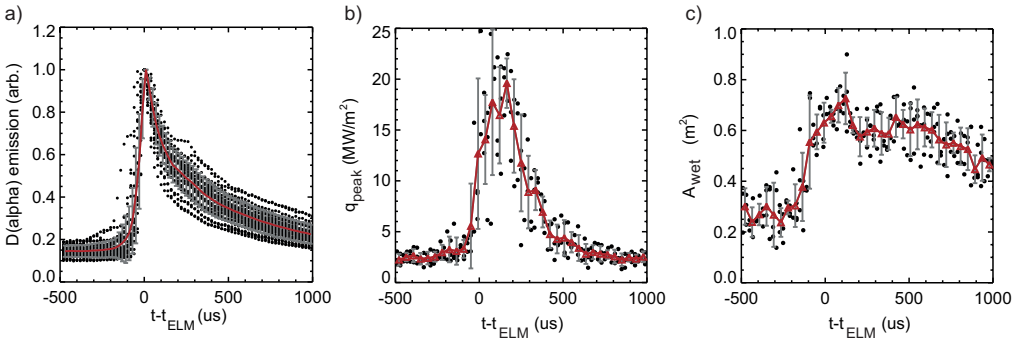

Figure 2. Panel a) shows the D_α temporal evolution from an average over 25 ELMs with the time normalised to the peak in the emission. Panel b) shows the corresponding ELM heat flux for the ELM, with the temporal evolution of the ELM wetted area shown in c). For all of the plots, the black circles represent the individual data points with a binned average shown by the solid red line for the case of a) and red line with triangles for b) and c). The variation in a given bin is given by the grey error bar.

During the peak of the heat flux the IR profiles are seen to exhibit several distinct maxima in the SOL part of the profile [21, 22]. Figure 3 shows a typical ELM profile at the peak of the ELM heat flux. The distinct maxima seen in the profile are seen to be caused by the arrival of the individual ELM filaments at the target, as confirmed using visible imaging [7]. The maxima can be used to extract information about the properties of the ELM such as the radial and toroidal filament diameters and mode number of the ELM filaments. The peaks are detected using a threshold on the signal level such that all peaks must have a magnitude greater than 15% of the peak heat flux in the profile with secondary maxima required to be 30% above the neighbouring local maxima. These thresholds on the profile level produce accurate identification of the peaks at the target, which can be seen in figure 3 where the maxima are identified using the red dot-dashed lines. Once the local maxima have been located, the minima around them can be found (blue long dashed line) and subsequently the half width, half maximum (HWHM) determined (grey horizontal lines).

The detection algorithm can be applied to each of the 25 ELMs in discharge 30378 and the temporal evolution of the number of maxima seen in the target profile, n_{fil}^{tgt}, as function of the time through the ELM cycle is shown in figure 4. The number of maxima in the target profile can be clearly seen to increase during the rise in the peak of the heat flux, although there is some variation from ELM to ELM in the location of the maximum number of striations seen at the target. The maxima in the profiles are generated by the arrival of filaments at the target, though it may be the case that a given filament extends more than once through the field of view of the IR camera. The correlation between the number of striations seen at the target and the ELM wetted

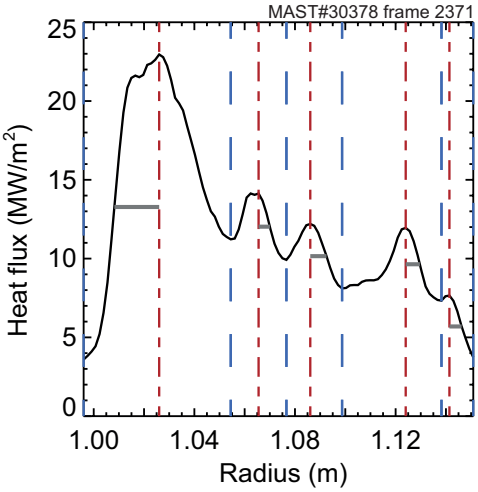

Figure 3. Detection of filament local maxima across an ELM profile taken at the peak of the ELM heat flux. The local maxima are marked by the red dot-dashed and the corresponding minima by the long dashed blue lines. The HWHM of the maxima are then indicated by the horizontal grey lines.

area, which both increase together, suggests that the arrival of the filaments at the target plays a role in the overall size of the ELM footprint [9, 14].

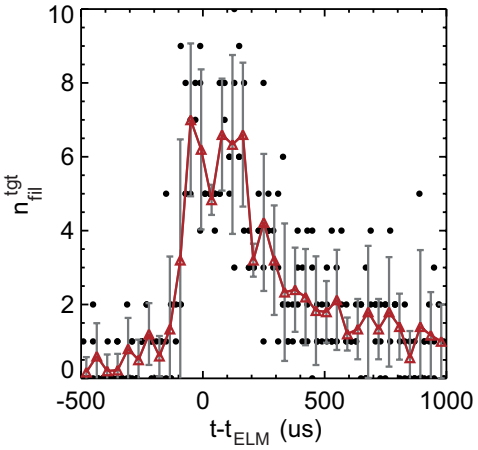

Figure 4. The number of local maxima corresponding to filaments, n_{fil}^{tgt}, as a function of time during the ELM averaged of 25 ELMs. The black points correspond to the individual ELM profiles with a binned average shown by the red line and triangles.

3. ELM database used for analysis of target data

The analysis of the single discharge shown in the previous section shows that the peak heat flux, wetted area and the number of striations at the target occur at similar times. Therefore, a database of lower single null and double null discharges has been generated by extracting the wetted area and the number of striations seen in the target IR data at the time of the peak ELM heat flux. The database allows the effect of the ELM

properties on the wetted area to be investigated. It is well known that there are several ELM types, each with different properties such as frequency, magnitude and mode number [23]. In this study, we restrict ourselves to type I ELMs, as these are observed to be the ELMs with the lowest toroidal mode number. On MAST, a good discriminator of ELM type is the electron temperature at the pedestal top, whereby type I ELMs are seen to have pedestal top temperatures above 100 eV [15]. The type I ELMs in the database are selected based on this threshold on the pedestal top temperature which is found using Thomson scattering [24] profiles of the plasma and performing a tanh fit to determine the pedestal parameters [25]. The parameters for a given ELM are taken in the last 20% of the ELM cycle. Application of this cut on the pedestal temperature produces a database of type I ELMs which consists of 84 LSN ELMs and 15 DND ELMs.

The analysis of the target footprints and timescales in LSN data can be complicated by the existence of secondary filaments that are a result of the interaction of the ELM filaments with coils or support structures inside the vessel [26]. The secondary filaments have been seen to extend the duration of the D_α decay at the midplane and the ion current at the target [26]. In order to understand what effect these secondary filaments have on the heat flux profiles, a comparison of the D_α duration and the duration of the target heat flux decay has been made between LSN and DND plasmas. The LSN data show longer D_α decays than the DND data, but both discharge types show the same heat flux duration at the target. This suggests that the secondary filaments do not carry a significant heat flux to the target and as a result do not affect the IR target profiles and analysis presented here.

4. Type I ELM wetted area and the number of target filaments

The variation of the wetted area as a function of ELM energy for type I ELMs for both LSN and DND discharges is shown in figure 5 a). Previous studies where all ELM types are considered has seen an increase in the ELM wetted area with the ELM energy [20, 16, 15]. However, when only one ELM type is considered the LSN data (black circles) show a weak dependence of the wetted area increasing with the stored energy which is within the scatter seen in the points. The variation in the wetted area at a fixed ELM energy is seen in a number of studies across multiple devices [27, 20] and suggests that the ELM energy is not the only factor in setting the ELM wetted area. The data from the DND discharges produces wetted areas that are generally smaller than the LSN data for a given ELM size and when considered alone there is a similar weak trend of increasing wetted area with ELM energy, though as with the LSN data, the scatter is significant. The difference in the wetted area between the LSN and DND data can be accounted for by the differing flux expansions between the two equilibria. The LSN data have flux expansions of the order 6.5, compared to typical value of 4 for the DND data. The wetted area, taking into account the flux expansion, is shown in figure 5 b). The figure shows that once the flux expansion is taken into account, the ELM wetted area across both types of plasma configuration are comparable.

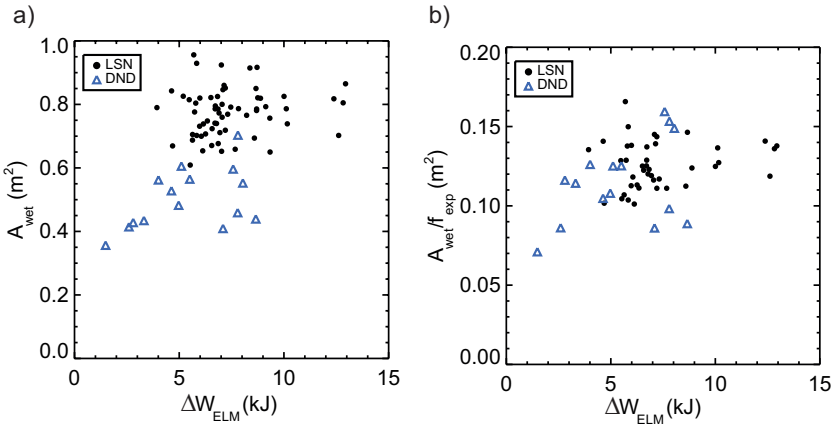

Figure 5. The calculated ELM wetted areas for type I ELMs shown in a), with the flux expansion removed in b), both as a function of ELM energy. LSN data is shown by the black circles and DND data by the blue triangles.

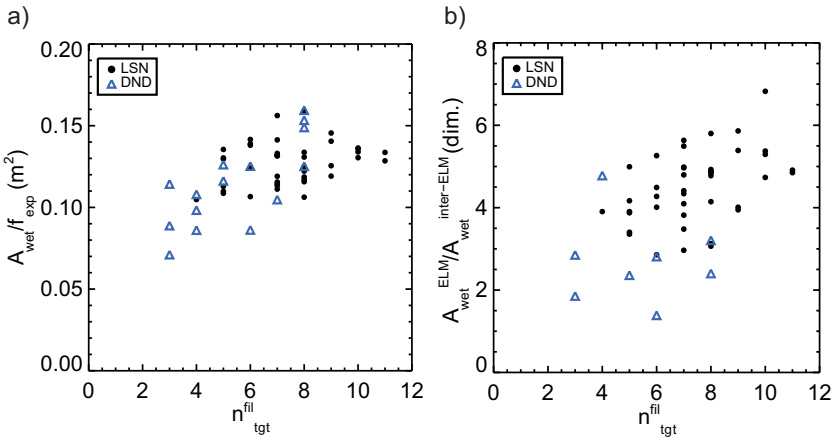

Figure 6. The ELM wetted area (panel a) corrected for flux expansion as a function of the number of filament peaks seen at the target is shown in a). The ratio of the ELM to inter-ELM wetted area as a function of the number of striations seen at the target for type I ELMs is shown in panel b). LSN data is shown by the black circles and DND data by the blue triangles.

The number of striations seen in the target ELM profiles, n^{fil}_{tgt}, is calculated as described in section 2 and varies during the ELM cycle as shown in figure 4. The variation of the wetted area with the number of striations or filaments in the target profile can then be investigated using the type I ELM database. Figure 6 a) shows the variation of the ELM wetted area with the number of striations seen in the target profiles with the flux expansion taken into account where all of the ELM parameters are extracted at the peak of the ELM heat flux. The black circles correspond to individual LSN ELMs and the blue triangles correspond the DND ELMs. The data shows that the wetted area increases with an increasing number of target filaments in both LSN and DND plasmas as both sets of data points follow a similar trend. The relationship between an increase in the number of striations at the target and an increase in the target

wetted area has also been seen in LSN ELMs on NSTX [14]. It is expected that a larger wetted area will give an increased number of filaments because of the mapping of the radial target size to the midplane toroidal angle [9, 16]. Profiles covering larger radial sizes will encompass larger toroidal angles at the midplane, and as such can capture more filaments. The scaling of the wetted area with the number of target striations is stronger than the scaling of the wetted area with the ELM energy, which suggests the number of filaments arriving at the target is dominant in setting the wetted area at a given point in the ELM cycle.

The ratio of the wetted areas is an ITER relevant quantity and includes the correction for the flux expansion which is taken to be the same for ELM and inter-ELM periods in a given ELM. The use of the ratio of the ELM to inter-ELM wetted area is used widely in these studies, but it does mix ELM transport and SOL transport which are governed by different mechanisms. It is likely that as the inter-ELM width scales as the inverse of the poloidal field and the plasma pressure scales as the square of the poloidal field, may result in larger broadenings for ITER but similar wetted areas. The scaling of the ELM/inter-ELM area as a function of n_{tgt}^{fil} is shown in figure 6 b) and show a similar trend to the wetted area data. The inter-ELM area in figure 6 b) has been generated using a parameterisation of the experimentally determined values. A parameterisation is used to generate a value for the inter-ELM area prior to a given ELM, this is used instead of the area calculated experimentally as significant scatter is seen SOL width studies which would affect the analysis of the ELM area. The parameterisation for the inter-ELM area depends on the plasma current as this has been seen to be the quantity which most affects the inter-ELM SOL width [28, 29]. The observed range for LSN data of $3 \leq A_{wet}^{ELM}/A_{wet}^{Inter-ELM} \leq 6$ is consistent with measurements from other machines where the upper limit seen is 6 [21, 27, 22]. The broadening seen in the DND data is smaller, with a range of $1 \leq A_{wet}^{ELM}/A_{wet}^{Inter-ELM} \leq 4$, which is at the lower end of the range required for successful ELM mitigation in ITER.

5. Relating the target filament number with the ELM mode number

The model of an ELM as a number of filaments travelling radially and toroidally away from the plasma edge has been seen to generate profiles at the target that are consistent with those seen experimentally [7]. If the number of filaments at the target plays a role in setting the ELM wetted area, then this would suggest that the ELM wetted area would also scale with the midplane toroidal mode number of the ELM. The spatial structure seen in the ELM profiles at the target can be used to determine the ELM midplane toroidal mode number by mapping the IR data to the midplane using the magnetic field, as previously performed on other machines [9, 11] and on L mode profiles in MAST [16].

5.1. Quasi toroidal mode number from IR data

The identification of the filament peaks in the target profiles allows the separation between the peaks seen in the target profiles to be determined. Figure 7 shows the variation of the filament separation in the IR profiles and the number of striations at the target. The data suggests that for both LSN and DND plasmas, higher numbers of filament peaks in the profile gives rise to a smaller spacing between the filaments at the target, though there is scatter about a given number of target filaments. The midplane quasi toroidal mode number (QMN) can be determined using the previously established relationship between the radial spacing at the target and the toroidal separation at the midplane [9, 16]. The quasi toroidal mode number is derived from an average toroidal distance between striations for the observed toroidal angle. High speed imaging shows that the filaments are equally spaced toroidally which is consistent with the variation seen in the distance between the striations [30].

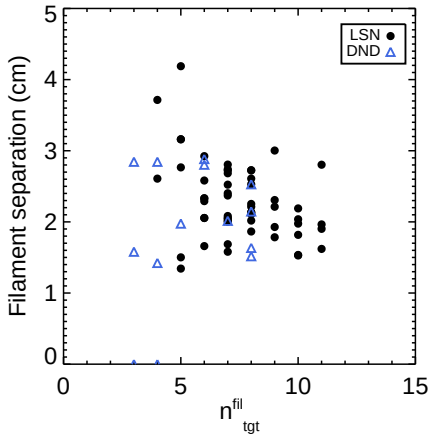

Figure 7. The radial separation between two filament peaks in the target profile as a function of the number of filament peaks detected. The data for the LSN plasmas are shown as black circles and the data for the DND plasmas are shown as blue triangles.

Once the location of the filament peak at the target is determined, field line tracing can be used to map the radial location at the target to the toroidal location at the midplane. Repeating the mapping for each of the filaments detected in a given ELM profile then allows the angular separation of the filaments at the midplane to be calculated. The quasi toroidal mode number (QMN) calculated using the filament spacing can then be used to estimate the ELM mode number from the IR target data. The QMN is calculated using the formula (taken from [9]);

$$QMN = \frac{1}{N}\sum_{i=1}^{N-1}\frac{2\pi}{\delta\phi_i} \tag{2}$$

where N is the number of striations analysed in a given ELM profile, $\delta\phi_i$ is the toroidal angle displaced at the midplane between the i^{th} and the $i^{th}+1$ filament. ELM

filaments located close to the strike point (within 5 cm of the LCFS) show a large sensitivity of the mapped midplane toroidal angle due to the large variation in connection length seen close to the X point. At the spatial resolution of the IR camera, the error on a given toroidal location within 5 cm of the LCFS is between 5 and 20 degrees. Therefore, assuming a typical mode number of n=10 and the corresponding error in the separation between two filaments at $\Delta R_{LCFS} = 5$ cm, the error on the calculated mode number would be 30%. The error decreases with increasing radius, with filaments at 10 cm from the strike point accurate to 10% in QMN.

The QMN calculated at the midplane is seen to lie in the range $5 \leq QMN \leq 25$, as shown in figure 8, with the peak of the distribution being in the range $QMN = 8 - 10$. The spread of values is larger than the error introduced by the mapping, justifying the use of only the data beyond 5 cm from the LCFS. In addition, the value for the wetted area can be affected by the time during the ELM cycle and the IR frame rate. The range and peak value of the QMN from the IR data are consistent with past analysis of the toroidal mode number calculated using midplane visible imaging in similar discharges [15]. Studies on JET also show the ELM QMN spanning the same range as the MAST data presented here, with the JET data showing little scaling with plasma parameters [31].

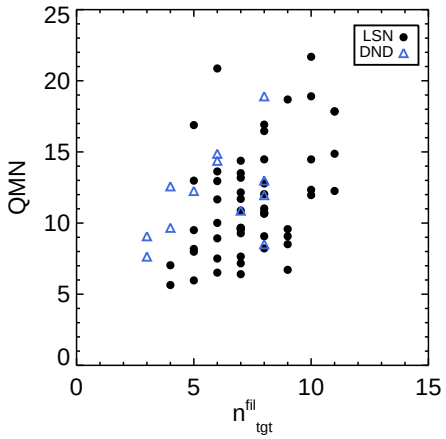

Figure 8. The calculated quasi toroidal mode number (QMN) along the abscissa against the number of striations seen in the IR target profiles on the ordinate for both LSN (black circles) and DND (blue triangles) plasmas.

The number of striations seen at the target generally maps to a higher toroidal mode number at the midplane, with the QMN being approximately 1.5 times larger than the observed number of target filaments. The discrepancy between these two quantities is expected as the filaments will not all deposit energy in the field of view of the IR camera (with the discrepancy suggesting that the toroidal coverage for the MAST data is 240 degrees), and there is variation in the departure time of the filaments which can affect the target pattern at the divertor by changing the arrival time of one filament relative to another [30]. The data shows that there is agreement in the range of toroidal mode

numbers seen for both LSN and DND plasmas.

Figure 9 a) shows the ratio of the ELM to inter-ELM wetted area as a function of the QMN calculated from the IR data. The data plotted in the figure is equivalent to the data in figure 6 b) and shows a trend of increasing ratio of ELM to inter-ELM wetted area with QMN. The increase in the ratio of the wetted areas arises from an increase in the ELM wetted area, as can be seen in figure 9 b) as both the flux expansion and the inter-ELM wetted are do not scale with the ELM QMN. The scaling of the wetted area is expected given the relationship between the QMN and the number of striations seen at the target shown in figure 8. The scaling of the wetted area with QMN is similar between both LSN and DND data when the flux expansion is taken into account.

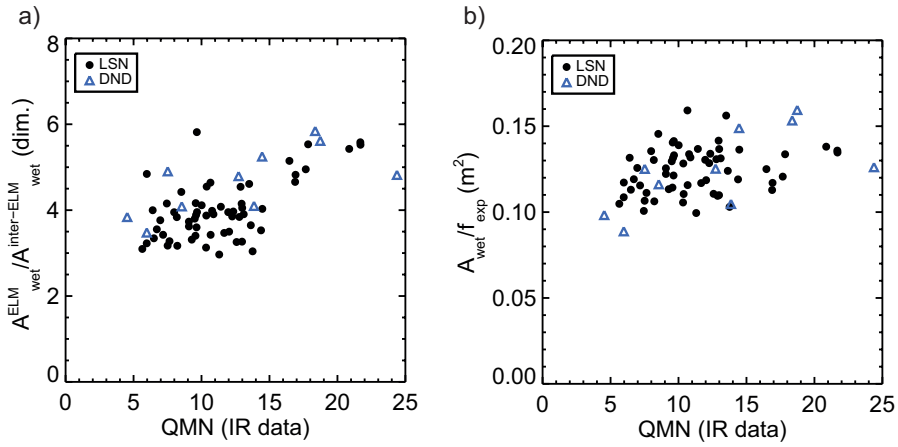

Figure 9. The variation of a) the target ELM to inter-ELM wetted area ratio with QMN and b) the ELM wetted area for both LSN and DND plasmas.

5.2. Quasi mode number from visible midplane imaging

The QMN calculated from the IR data can be compared to data from midplane visible imaging to investigate if the toroidal mode number at the midplane affects the wetted area of the ELM. Ideally, visible midplane imaging would be available for the data shown in figure 9 a), however, the analysis of the visible imaging data to determine the mode number requires high speed visible imaging ($>$ 10 kHz frame rate) of the ELM cycle to identify the mode number which is not available for the shots shown above. However, a selection of high speed imaging data is available for DND discharges which are similar to the data in the IR database, yielding 65 type I ELMs which can be analysed for the visible mode number. The IR wetted area for these shots can be calculated using lower spatial resolution IR data (5 mm per pixel), but the number of striations at the target cannot be accurately determined using the lower spatial resolution IR data.

The QMN from the visible data is obtained by taking a field line generated at the plasma edge and extracting the pixel intensity at each point along it. If the intensity is plotted as a function of the toroidal angle at which the field line is overlaid onto the image, filaments that align to the field line correspond produce large line integrals and

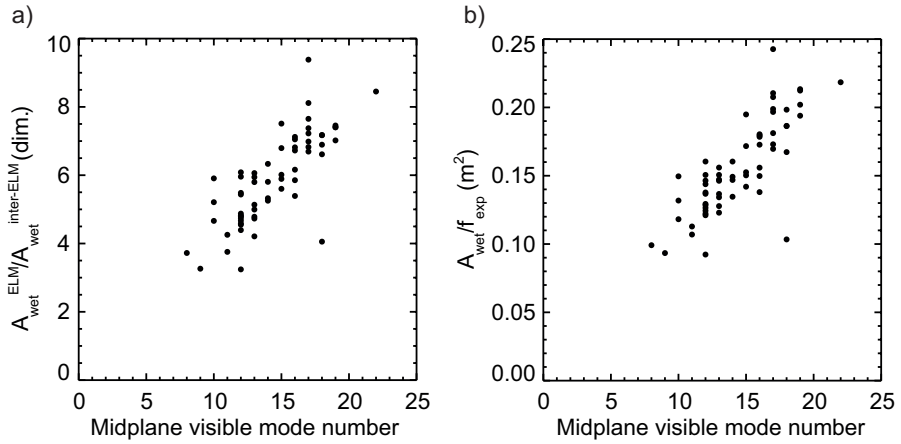

Figure 10. a) The lower outer divertor ELM to inter-ELM wetted area as a function of the quasi mode number derived from visible data in double null discharges. b) The lower outer divertor ELM wetted area as a function of the quasi mode number derived from DND visible imaging.

allow the toroidal angle at which the filaments are located to be identified [18]. The visible imaging data is taken during the rise time of the midplane D_α before the filaments separate from the LCFS and prior to the production of any secondary filaments which could affect the mode number. The QMN is then calculated by applying equation 2 to the resulting spacing between the filaments. The visible QMN for the type I ELMs analysed is shown in figure 10 a) against the target ratio of ELM to inter-ELM wetted area calculated from the IR measurements. The typical visible mode number is in the range n=10-20 which is consistent with past analysis of DND and LSN ELMs [30, 15] and of the values calculated from the target IR data. As for the case of the IR data, the increase in the ratio of the wetted areas is generated due to an increase in the ELM wetted area (figure 10 b), with the inter-ELM wetted area and flux expansion not showing a scaling with the mode number.

The QMN from the IR data and the visible data are within the same range, as shown in figure 11, where the peak value is similar for both, though the visible data shows a higher upper limit on the mode number. The higher visible mode number compared to the value calculated by the IR data is consistent with the restricted field of view of the IR compared to the visible as discussed previously. The overlapping ranges in the dataset used for the IR analysis of the QMN and the visible QMN supports the argument that discharges in both datasets are similar and shows that there is a relationship between the midplane mode number, number of striations at the target thought to be from the arrival of filaments and the wetted area at the divertor. The wetted area over the two datasets are similar, with a larger range of values in the visible data case. The relationship between these quantities is such that increasing midplane the mode number leads to an increased wetted area at the target from the ELM filaments.

Recent ITER predictions have used the observed range of $3 \leq A_{wet}^{ELM}/A_{wet}^{Inter-ELM} \leq 6$ to estimate the level of mitigation required for ITER [3]. The ITER prediction when

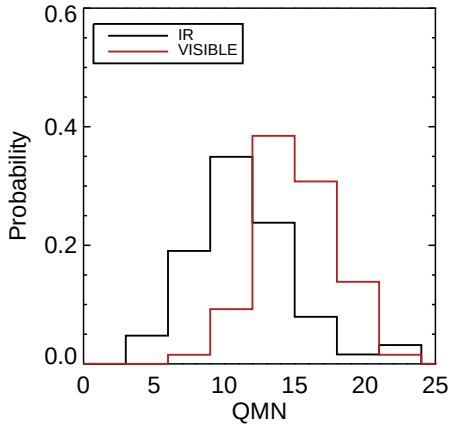

Figure 11. QMN calculated using the IR data and the visible data for discharges with similar plasma characteristics.

the ratio is 1, a minimum ELM frequency of 45 Hz is required to control the ELMs and reduce them to a tolerable level. The broadening seen in the MAST data, which is consistent with current predications, if it applies to ITER, would allow controlled ELMs at frequencies of between 7 and 15 Hz, which is consistent with the level of mitigation currently assumed for ITER [3]. However, this is based on the assumption that the ELMs in ITER are driven unstable by the same mechanism as seen in MAST. If the ITER ELMs are peeling unstable, as suggested by modelling [32] then the ELM mode number will be lower than that seen on MAST. As the trend from the MAST data is a decreasing amount of broadening with ELM mode number, in agreement with NSTX [14], this would suggest less broadening on ITER than MAST which would affect the level of ELM control required. It also assumes that there is a linear reduction in the ELM heat flux with ELM frequency, which is not observed to be true as the heat flux is typically observed to fall at a lower rate than the reduction in the ELM energy [27, 20]. Therefore, a key issue for assessing the ELM wetted area in ITER is predicting what the expected ELM mode number will be.

6. ELM filament modelling

The experimental data show an effect of the toroidal mode number of the ELM on the strike point footprint, however, there is a significant level of scatter in the data and this is seen not only in MAST data, but also in data from other machines [27]. In order to better understand the target profiles during ELMs, modelling can be performed using a Monte Carlo simulation [7] whereby a filament of fixed radial and toroidal size is followed as a function of time while it propagates through the magnetic field with a given toroidal and radial velocity. The particles in the filament have a Gaussian distribution about the filament centre and are assigned a Boltzmann temperature distribution. The model only tracks ions and the ion temperature is taken to be 100 eV corresponding to the pedestal

top electron temperature and assuming that the ion and electron temperature are equal in the pedestal. The mapping of the particle location through the magnetic field from the midplane to the target is performed using a parameterisation of the magnetic field obtained through field line tracing, which is described in Kirk et al [7]. The modelling described here uses the magnetic equilibrium of a 400 kA LSN discharge for all cases. The diameter of the filaments in the toroidal direction, perpendicular to the field line, is 10 cm and the diameter in the radial direction is 7 cm. These parameters are set to produce a target profile that is representative of the IR measurements.

Experimentally, the ELM filaments are seen to remain stationary at the plasma edge for a certain period of time and then separate from the LCFS. Following the separation of the filaments from the plasma edge they decelerate toroidally whilst accelerating radially out into the SOL. The dwell time at the plasma edge is taken to be 200 μs and this is determined by matching the heat flux rise time in the modelling with that from experiment. There is a random time offset of $\pm$ 25 μs added to the separation time as spread of separation times is seen experimentally [7]. The acceleration of the filaments in the toroidal and radial direction is assigned for a given filament with the value for the acceleration derived from experimental measurement; the radial acceleration 1x10^8 ms^{-2} and the toroidal deceleration is centred on -3x10^8 ms^{-2} [7]. Each of the particles in the filament are then followed until they strike the divertor surface when the location and time of arrival is recorded. The IR profiles are simulated by selecting all of the particles that arrive in a radial segment of the target and binning according to the time of arrival. The size of the time bin of 30 μs is chosen to reflect the integration time of the recorded IR data.

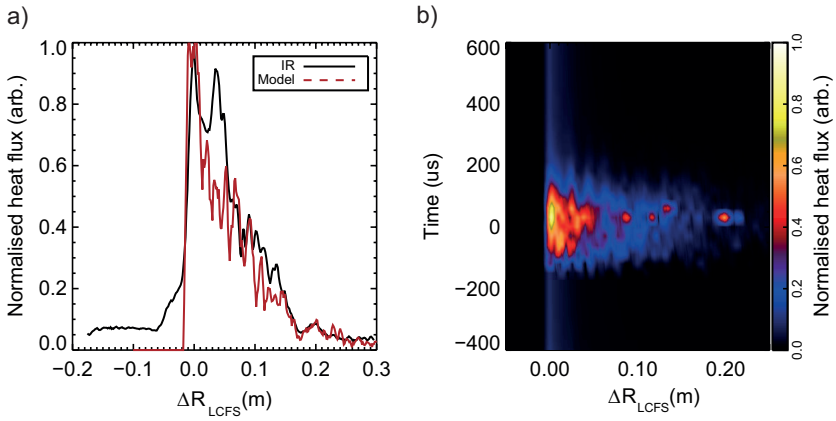

Figure 12. a) A modelled ELM profile at the target (red line) compared to the measured ELM heat flux (black solid line). b) Contour plot of the spatial and temporal evolution of the ELM at the target to show the obvious similarities between the modelled data and the IR measurements. The time axis is normalised to the peak of the heat flux.

In general, these parameters are adjusted to give a good match to the experimental profiles and timescales seen during the ELMs. A comparison of the modelled profile with an experimentally measured one is shown in figure 12 a) and it can be seen that the

overall shape and randomly located filaments can be seen and are consistent across both modelled and experimental profiles. The temporal evolution of the heat flux is shown in 12 b) and is consistent in terms of temporal evolution of the heat flux experimentally (as shown in figure 1 a)). The wetted area is calculated by using the same technique as used for the IR data. A steady state background profile with peak heat flux 10% of the ELM peak and of width $\lambda_q = 5$ mm at the midplane is added onto the data to represent the inter-ELM heat flux as the model only recreates the heat flux from the ELM. Further refinement of the model could be made to make an exact match, however, it is expected that the target profile will vary from ELM to ELM and with toroidal angle. As such the general agreement seen between modelling and experiment shows that the model accurately captures the ELM effects on the target profiles.

The first test of the model is to investigate the effect of the ELM mode number on the number of striations seen at the target. Modelling using input mode numbers of n=5, 10, 15 and 20 is used to generate target profiles, which are then analysed using the peak detection applied to the experimental data. The location of the peaks can then be converted, as with the experimental data, into a midplane QMN using a mapping between the target radius and the midplane toroidal angle. Figure 13 shows a comparison between the modelled midplane mode number and the QMN returned from the modelled profiles. The modelling supports the experimental data where a positive scaling between the number of target filaments and the midplane mode number is seen. The modelling also shows the QMN is lower than the actual ELM mode number, consistent with the interpretation of filaments at different toroidal locations not fully extending into the field of view of the IR camera or are not detected due to the target profile resolution used.

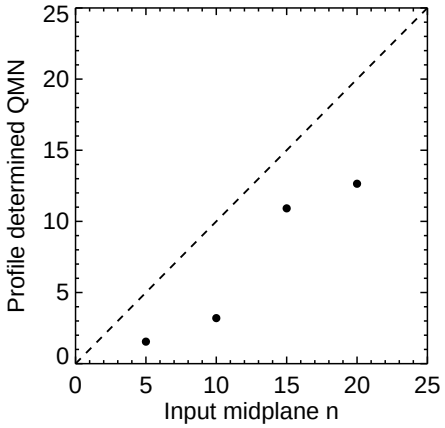

Figure 13. Comparison of the input mode number to the model and the QMN calculated using the modelled profile and peak detection.

The modelled target footprint is available for all toroidal angles at the target at any point during the ELM cycle, unlike the IR measurements where only one toroidal location can be measured. The availability of all the toroidal information allows the

variation of the profile to be investigated for the same upstream ELM conditions. A sample of 150 toroidal locations are taken, evenly spaced from the full toroidal footprint obtained from the model. Selecting these locations allows the effect of the toroidal angle on the wetted area to investigated for the same ELM. The result shows that the wetted area exhibits scatter about an average value, as is seen experimentally. Figure 14 a) shows how this toroidally averaged wetted area changes as the number of ELM filaments in the simulation is increased, whilst keeping the fraction of particles in a filament constant. The error bars represent the standard deviation of the wetted area returned by the model as a result of taking profiles at different toroidal angles.

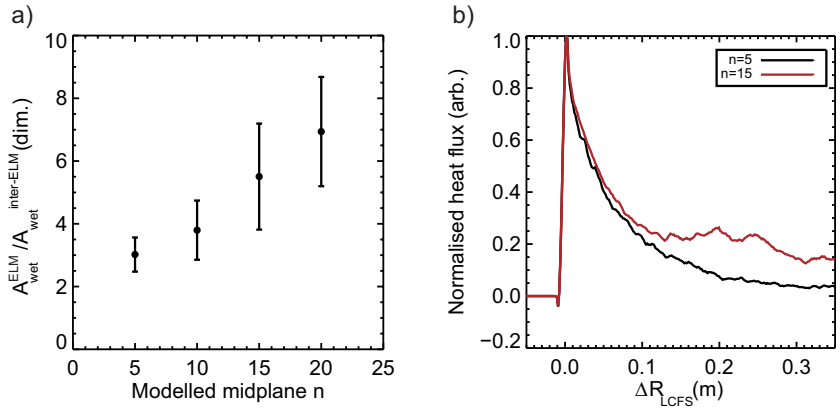

Figure 14. The modelled target wetted area represented by the ratio of the ELM to inter-ELM wetted areas averaged over 150 toroidal locations for a fixed ELM energy and a varying number ELM toroidal mode number is shown in panel a). The error bars are the standard deviation on the mean of the data. Panel b) shows a comparison of the toroidally averaged modelled ELM profiles at the peak of the heat flux for ELMs for two different ELM toroidal mode numbers.

There is a trend of increasing wetted area with toroidal mode number, which is consistent with the experimental data shown in figure 9 a) and supports the observation that the QMN affects the wetted area at the target. For each of the modelled cases with a different toroidal mode number, a profile can be generated from the modelled data to see what effect the changing mode number has on the profile shape. Figure 14 b) shows two profiles extracted from the modelling using a toroidal mode number of n=5 and 15 where the profiles have been averaged over all toroidal locations to assess the impact of increasing the ELM mode number on the profile width. It can be seen from the figure that the increase in the toroidal mode number of the filaments carries more particle outwards, in effect broadening the profile and giving rise to the increase in the wetted area. The variation about the average wetted area for a given mode number, as denoted by the error bars in figure 14 a) arises from the toroidal variation of the footprint which is averaged out of the profiles in b). The toroidal variation of the ELM footprint can be seen in figure 15 which shows the modelled target heat flux for two n=5 cases at the peak of the modelled heat flux. There is variation in the width of the footprint as a result of the individual filaments arriving at the target at different times and this produces

the variation in the wetted area which is seen experimentally. The analysis presented here can point to some causes of the variation in the wetted area, but is limited in that for a full understanding a large range of simulations would be required that varied the separation time and acceleration of the filaments systematically to generate sufficient statistics.

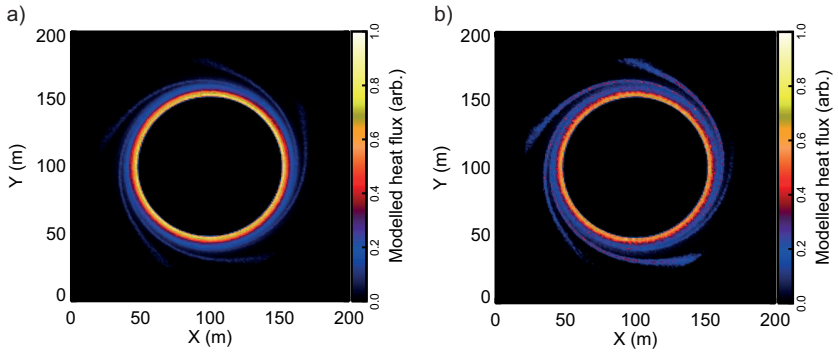

Figure 15. The modelled footprint at the divertor from a) a set of filaments that separate from the plasma edge simultaneously and accelerate at the same rate and b) for a set of filaments with a variable separation time and acceleration.

7. Conclusion

The heat flux due to ELMs is a key issue for ITER due to the limitations that it places on the lifetime of the divertor. The peak heat flux deposited to the target depends on a number of ELM parameters, one being the area over which the energy is deposited, the understanding of this effect is the aim of this paper. Through the use of data from MAST, it has been seen that there is significant broadening of the target footprint during the ELM which can be characterised by the ELM wetted area. Data from composite ELMs shown that the wetted area peaks at the maximum ELM heat flux and during the ELM the target footprint exhibits several striations which are generated by the arrival of individual filaments at the target. Through the generation of a database, the variation of the wetted area with ELM energy for the type I ELMs analysed is seen to be weak, but there is a clear dependence of the wetted area and the number of striations seen in the target profiles. The rising wetted area with the number of striations seen at the target suggests that the filaments play a role in setting the size of the ELM target footprint. The ELM wetted area is seen to vary between 3 to 6 times the inter-ELM width for LSN plasmas, which is greater that then used in ITER predictions. However, the data shows that the ratio of the ELM to inter-ELM wetted area decreases with toroidal mode number, and it is suggested that low collisionality ITER pedestal will be peeling unstable and as such will have lower mode numbers, and correspondingly less broadening, than the MAST ELMs analysed here. Therefore, a key area of future research is the factors affecting the ELM mode number and the effect the pedestal stability has on determining this value.

The ELM quasi toroidal mode number can be calculated from the target data, and from visible imaging. The analysis presented here has shown that the mode number calculated using both of these methods generates a similar value, with the IR data giving an underestimate. The cause of this underestimate is likely due to the limited toroidal view of the IR camera, and that not all of the filaments extend into the field of view of the IR camera. The positive scaling of the midplane mode number and the ELM to inter-ELM ratio is seen and is similar in both the IR and visible data, though the mechanism that sets the ELM mode number is not understood and should be the focus of future work. The use of a Monte-Carlo model has contributed to the understanding of the experimental data, replicating the variation of the wetted area for a given ELM due to toroidal variation and showing a trend of increasing ELM wetted area with input midplane mode number. The use of simulations with variable filament separation times has been seen to give the best agreement to the experimental data, and is consistent with visible imaging which shows a period over which the filaments separate [7].

Acknowledgments

This work has been carried out within the framework of the EUROfusion Consortium and has received funding from the Euratom research and training programme 2014-2018 under grant agreement No 633053 and from the RCUK Energy Programme [grant number EP/I501045]. To obtain further information on the data and models underlying this paper please contact PublicationsManager@ccfe.ac.uk. The views and opinions expressed herein do not necessarily reflect those of the European Commission.

References

[1] PT Lange et al. ELM control strategies and tools: status and potential for ITER. *Nucl. Fusion*, 53:043004, 2013.

[2] G Federici et al. Assessment of the erosion of the ITER divertor targets during type I ELMs. *Plasma Phys. Control. Fusion*, 45:1523–47, 2003.

[3] A Loarte et al. Progress on the application of ELM control schemes to ITER scenarios from the non-active phase to DT operation. *Nucl. Fusion*, 54:033007, 2014.

[4] A Kirk et al. Evolution of filament structures during edge-localized modes in the MAST tokamak. *Phys. Rev. Lett.*, 98:185001, 2006.

[5] HR Wilson et al. Theory for explosive ideal magnetohydrodynamic instabilities in plasmas. *Phys. Rev. Lett.*, 92:175006, 2004.

[6] S Saarelma et al. MHD and gyro-kinetic stability of JET pedestals. *Nucl. Fusion*, 53:123012, 2013.

[7] A Kirk et al. Evolution of the pedestal on MAST and the implications for ELM power loadings. *Plas. Phys. Control. Fusion*, 49:1259–75, 2007.

[8] T Eich et al. Nonaxisymmetric energy deposition pattern on ASDEX Upgrade divertor target plates during Type-I edge-localized modes. *Phys. Rev. Lett.*, 91:195003, 2003.

[9] T Eich et al. Type-I ELM substructure on the divertor target plates in ASDEX Upgrade. *Plasma Phys. Control. Fusion*, 47:815, 2005.

[10] JH Yu et al. Fast imaging of edge localized mode structure and dynamics on DIII-D. *Phys. Plasmas*, 15:032504, 2008.

[11] S Devaux et al. Type-I ELM filamentary heat load patterns on the divertor target at JET. In *36th EPS Conference on Plasma Phys. Sofia ECA Vol.33E, P-2.157*, 2009.

[12] A Wingen et al. Numerical modelling of edge-localized-mode filaments on divertor plates based on thermoelectric currents. *A Wigen and others*, 104:175001, 2010.

[13] G Huijsmans and A Loarte. Non-linear MHD similation of ELM energy deposition. *Nucl. Fusion*, 53:123023, 2013.

[14] JW Ahn et al. Broadening of divertor heat flux profile with increasing number of ELM filaments in NSTX. *Nucl. Fusion*, 54:122004, 2014.

[15] A Kirk et al. Effect of resonant magnetic perturbations on low collisionality discharges in MAST and a comparison with ASDEX-Upgrade. *Nucl. Fusion*, 55:043011, 2015.

[16] AJ Thornton et al. The effect of L mode filament on divertor heat flux profiles as measured by infrared thermography on MAST. *Plasma Phys. Control. Fusion*, 57:115010, 2015.

[17] A Herrmann et al. Limitations for divertor heat flux calculations of fast events in tokamaks 27th conf. to plasma physics and controlled fusion (Madeira, Portugal). In *Proc. EPS 2001*, 2001.

[18] A Kirk et al. Filamentary structures at the plasma edge on MAST. *Plas. Phys. Control. Fusion*, 48:B433–B441, 2006.

[19] S Jachmich et al. Power and particle fluxes to plasma facing components in mitigated ELM H-mode discharges on JET. *J. Nucl. Mater.*, 415:S894–S900, 2011.

[20] AJ Thornton et al. Divertor heat fluxes profiles during mitigated and unmitigated ELMs on MAST. *J. Nucl. Mater.*, 438:S199–S202, 2013.

[21] M Jakubowski et al. Overview of the results on divertor heat loads in RMP controlled H-mode plasmas on DIII-D. *Plasma Phys. Control. Fusion*, 49:095013, 2009.

[22] T Eich et al. Type-I ELM power deposition profile width and temporal shape in JET. *J. Nucl. Mater.*, 415:S856–9, 2011.

[23] H Zohm et al. Edge localised modes (ELMs). *Plasma Phys. Control. Fusion*, 38:105–128, 1996.

[24] R Scannell et al. Design of a new Nd:YAG Thomson scattering system for MAST. *Rev. Sci. Inst.*, 79:10E730, 2008.

[25] RJ Groebener and TN Carlstrom. Critial edge parameters for H-mode transition in DIII-D. *Plasma Phys. Control. Fusion*, 40:673, 1998.

[26] S Elmore et al. Scrape off layer ion temperature measurements at the divertor target during type III and type I ELMs in MAST measured by RFEA. *Plasma Phys. Control. Fusion*, 58:065002, 2016.

[27] H Thomsen et al. Power load characterisation for type-I ELMy H modes in JET. *Nucl. Fusion*, 51:123001, 2011.

[28] T Eich et al. Scaling of the tokamak near the scape-off layer in H-mode power width and implications for ITER. *Nucl. Fusion*, 53:093031, 2013.

[29] AJ Thornton et al. Scaling of the scrape off layer width during inter-ELM H modes on MAST as measured by infrared thermography. *Plasma Phys. Control. Fusion*, 56:055008, 2014.

[30] N Ben Ayed et al. Inter-ELM filaments and turbulent transport in the Mega Amp Spherical Tokamak. *Plas. Phys. Control. Fusion*, 51:035016, 2009.

[31] S Devaux et al. Type-I ELM filamentary substructure on the JET divertor target. *J. Nucl. Mater*, 415:S865–8, 2011.

[32] PB Snyder et al. A first principles predictive model of the pedestal height and width: development, testing and ITER optimisation with the EPED model. *Nucl. Fusion*, 51:103016, 2011.